Geomechanics for Energy and the Environment 35 (2023) 100487

Contents lists available at ScienceDirect

Geomechanics for Energy and the Environment

journal homepage: www.elsevier.com/locate/gete

A hydro-mechanical semi-analytical framework for hollow cylinder sanding tests

Panayiotis Kakonitis [a], Elias Gravanis [b,c], Ernestos N. Sarris [a,*]

[a] Department of Engineering, Oil and Gas Program, University of Nicosia, Nicosia, CY-1700, Cyprus
[b] Department of Civil Engineering and Geomatics, Cyprus University of Technology, Limassol, CY-3036, Cyprus
[c] Eratosthenes Centre of Excellence, Cyprus University of Technology, Limassol, Cyprus

ARTICLE INFO

Article history:
Received 15 February 2023
Received in revised form 11 June 2023
Accepted 10 July 2023
Available online 13 July 2023

Editors-in-Chief:
Professor Lyesse Laloui and Professor Tomasz Hueckel

Keywords:
Sand production
Hydrodynamic erosion models
Degradation laws
Elastoplasticity
Hollow cylinder

ABSTRACT

In this work we propose a novel semi-analytical hydro-mechanical framework for modeling sand production in the context of the hollow cylinder test, based on a kinematic formulation of the hydro-mechanical models of Vardoulakis et al. (1996) and Papamichos et al. (2001). We aim at the construction of a simple and useful tool which allows for quick estimates of the relevant quantities and can be efficiently used to study different forms of the postulated laws regarding the mechanics, hydrodynamics and degradation of the rock. In particular, this framework can be used to systematically calibrate the sand production coefficient λ as a function of the external conditions of the experiment, such as the external stress, which still is a major unknown in the hydro-mechanical modeling of the erosion process. As a first approximation we restrict ourselves to the case where pressure drawdown is small compared to the external stress, which is applicable in certain laboratory experiments. We illustrate the application of the framework by studying the effect of different forms of the hydrodynamic law, modified in the low porosity regime and the degradation law with respect to the non-linear dependence of cohesion and friction angle on the porosity. We use this framework to calibrate the dependence of λ on the external stress using the data of the experiment of Papamichos at al. (2001). We find that the sand production coefficient exhibits a power law modified by a decreasing exponential dependence as has been suggested in a recent work by the authors. The model is also applied in a different sanding experiment with varying external stress and flow rate exhibiting good agreement with the laboratory dataset.

© 2023 Elsevier Ltd. All rights reserved.

1. Introduction

A significant percentage of the world's hydrocarbons are hosted in consolidated and unconsolidated sandstone reservoirs which are prone to sand production after some time from the beginning of production. Sand production is the process by which particles from oil and gas wells are produced together with hydrocarbons after the particles detach from the host reservoir rock due to erosion. These particles migrate from the eroded surface of the rock and carried away from the well's inner surface by the produced reservoir fluids. The risk of sand particles being produced from weak rock reservoirs is quite high, if the pressure drawdown is also high. When the erosion process onsets, it creates operational problems, elevates the operational cost-economics of the producing company, creates discontinuous production of hydrocarbons because of expensive workovers, as well as health and safety issues. For these reasons, companies are continuously seeking solutions or invest funds in the understanding of the mechanisms escalating sand production in order to mitigate these unwanted problems that eventually may lead to catastrophic failures. Another significant issue that arises from solids production is their disposal in the environment. The particles are contaminated with hydrocarbons and their cleaning process before dumping them in stockpiles may become economically unaffordable or spend funds at the order of billions per annum for preventive measures. In general, sand production is investigated with models based on field or experimental observations often calibrated by field or laboratory data to prove their predictive efficiency. Research works on numerical, analytical and experimental investigations include: Qiu et al.,[1] Osisanya,[2] Papamichos,[3] Rahmati et al.,[4] Volonte et al.,[5] Ikporo and Sylvester,[6] Wang and Sharma,[7] Gravanis et al.,[8,9] Gholami et al.,[10] Li et al.,[11] Eshiet et al.,[12] Fetrati and Pak,[13] van den Hoek et al.,[14] Subbiah et al.,[15] Sarris et al.,[16] Ma et al.,[17] Zhang et al[18] and Kakonitis et al[19]

Many researchers have attempted to explain the cause of sand production. Sanding is attributed to the increase of effective

* Corresponding author.
E-mail addresses: kakonitis.p@live.unic.ac.cy (P. Kakonitis), elias.gravanis@cut.ac.cy (E. Gravanis), sarris.e@unic.ac.cy (E.N. Sarris).

https://doi.org/10.1016/j.gete.2023.100487
2352-3808/© 2023 Elsevier Ltd. All rights reserved.

Nomenclature

Greek symbols

λ	Sand production coefficient
Λ	Plastic zone depth
ϕ	Porosity field
ϕ_0	Initial porosity
$\overline{\phi}$	Mean porosity within the plastic zone
Φ	Friction angle of the rock
Φ_0	Initial friction angle
σ_r	Radial stress
σ_θ	Tangential stress
σ_{out}	External radial stress
ρ_s	Mass density of the rock

Latin symbols

a_D	Rate of softening (Eqs. (25) and (26))
a_H	Exponent in hydrodynamic constitutive Eq. (24)
C	Cohesion of the rock
C_0	Initial cohesion
H	Height of the hollow cylinder
q	Darcy flux
Q	Volumetric flow rate
r	Radial distance from the cylinder axis
r_{in}	Inner radius of the hollow cylinder
r_{out}	Outer radius of the hollow cylinder
S_0	Uniaxial compressive strength
u	Speed of advancement of plastic yielding

stresses from a series of events like (i) the stress redistribution in the rock due to drilling and perforation activities, with the latter being the communication between the well and the reservoir, (ii) high pressure gradient or drawdown when production starts and (iii) reservoir depletion after few years. The aforementioned physical processes are responsible for increasing the effective stresses in the near area of the wellbore creating structural damage of the rock, micro-fractures, and degradation of the rock formation by reduction of the cohesion and the friction angle. Therefore, the root cause of sanding can be attributed to (a) rock formations (unconsolidated or weakly consolidated), (b) type of bottom hole completion used e.g. cemented and perforated or barefoot wells, and (c) pressure manipulation strategies for production maintenance to a desired flow rate.[4,20–24]

A wide range of modeling approaches have been proposed to account for sand production. Models based on hydrodynamic erosion law which may be coupled with mechanical processes has been proposed by Vardoulakis et al.,[25] Stavropoulou et al.,[20] Papamichos et al.,[21] Fjaer et al.,[26] Detournay[27] and Le Pense.[28] Purely hydro-dynamical analytical models have also been recently put forward, see e.g. Ref. 29. Given that rock degradation and/or failure is regarded as a prerequisite for sanding, the majority of models with hydro-dynamical and/or mechanical nature associate erosion with localized deformations. For example, the formation of shear bands can be regarded as a key phenomenon inducing sanding, see e.g. Refs. 30, 31. The theory that localized deformation is one of the reasons of erosion onset has been already put forward by Papamichos et al[21] relating the onset and the rate of the erosion with the local magnitude of plastic strain. Models with primarily mechanical nature based either on tensile or shear failure criteria were proposed in the past by Bratli and Risnes[32] and Morita et al[33] but also more recently by Nouri et al[22] Finally, an erosion model based on strength mobilization was also proposed by Li et al[34]

The present work is concerned with the formulation of a simple semi-analytical framework for modeling sand production based on a hydro-mechanical description of erosion according to the following assumptions: (i) erosion occurs within the yielded region of the rock, (ii) erosion is governed by a hydro-dynamical law, (iii) the rock undergoes softening in the yielded zone according to a predefined degradation law. The yield criterion used is the usually adopted Mohr–Coulomb suit for modeling shear failure. It is well known, see e.g. Ref. 35, that sanding may not be directly related to yielding of the rock, but rather related to the magnitude of strain.[36] Nonetheless, the crudeness of our assumptions is justified by our intention to build an easy to formulate but effective tool for quick estimates regarding sand produced, utilizing the symmetry of the hollow cylinder laboratory test. Within the proposed context, one may examine a wide range of hydro-dynamical erosion and degradation laws, based on empirical information and conceptual choices, to reach an effective prediction of sand production of various rock types at laboratory scale. Moreover, it allows one to calibrate the sand production coefficient λ, for any given material, for different values external stress, which is a major unknown in any formulation of the hydro-mechanical modeling of erosion. This is in fact an important motivation for the present work.

Specifically, the proposed framework builds on our previous contribution[37] reducing the description of the erosion process in the progression of the plastic zone depth and the mean porosity within the zone. The plastic zone depth is determined by equilibrium which is used quasi-statically while mean porosity evolves by an equation deduced from the chosen hydro-dynamical erosion law. We further elaborate on these ideas and apply them as a framework in modified non-linear degradation and erosion laws. The degradation law needs also to be employed to account for the softening of the rock due to erosion. Owing to the cylindrical symmetry of the experimental test and our simplifications, the mathematical analysis of the problem leads to a pair of ordinary differential equations for the two basic dynamical variables, which are integrated numerically in a straightforward manner. Moreover, following Gravanis et al.,[37] in order to reduce the mathematical description to its simplest form, we restrict ourselves to experimental situations where pressure drawdown is quite small compared to the externally applied stress. We perform a parametric study of the hydro-dynamical erosion and degradation laws and deduce and evaluate the effect of the different forms on the characteristics of the sand production process, that is, the mass production, porosity, kinematics of the plastic zone depth as functions of time, expressing everything in suitable dimensionless form.

Additionally, we set the obtained models against two different experimental datasets where the drawdown pressure is negligible relatively to the applied stresses. Comparison with the tests of Papamichos et al[21] allows us to calibrate the sand production coefficient as a function of external stress for the different constitutive laws and obtain a good agreement with the trend of experimental sand production. The aforementioned dependence is fitted by a modified power law with decreasing exponential factor, building on our previous work.[19] By suitably modeling the geometry and stress conditions of the experiment of Kooijman et al.,[38] we apply our framework to a case with continuously variable external stress and variable flowrate obtaining good agreement with measured sand production.

This work is organized as follows. In Section 2 we present the mathematical formulation of the novel framework, in Section 3

we present the results of the analysis of the chosen hydrodynamical erosion and degradation laws and the comparisons with experimental tests, and in Section 4 we discuss and evaluate the main findings of this work.

2. Mathematical model

The aim of the proposed model is to simplify the hydrodynamic type of erosion models to the bare minimum, in order to clarify the workings of the mechanisms involved i.e., (i) plastic yielding, (ii) erosion and (iii) degradation, as much as possible. At the same time, we investigate at greater depth the effects of degradation and hydro-dynamic erosion models through a suitable family of models. The modeling of the physical problem of erosion involves two main processes: (a) response of the rock under poro-mechanical conditions and (b) the erosion process that takes place the inner surface of the hollow cylinder rock sample. The first process follows principles from the theory of poroelastoplasticity, while the second can be formulated along the lines of the seminal sanding model of Vardoulakis et al[25] which was later extended by Papamichos et al[21] and Gravanis et al[8] by proposing a novel semi-analytical formulation of the erosion problem as applied to the hollow cylinder test.

As explain earlier, our focus turns to the simplified geometry of the standard hollow cylinder test which allows for a conceptual re-visit of the governing equations of the problem at hand. In the context of this test, the sample is assumed homogeneous and saturated by a single-phase fluid. In the proposed model, the necessary dynamical variables to describe the evolution of erosion are reduced to the plastic zone depth and the mean value of the porosity within the plastic zone. These two quantities are merely functions of time. Therefore, the governing equations of the proposed model take the form of a pair of ordinary differential equations constructed by the following mechanisms: (i) The plastic zone depth is determined in a quasi-static manner by the continuity of the stress field across the plastic zone boundary as proposed by Gravanis et al[8] but introducing the simplification that the effect of the pressure can be regarded as negligible. The reason behind this assumption is the observation that in certain experimental cases presented by Papamichos et al.,[21] the fluid pressure is nearly two orders of magnitude smaller than the applied stress. (ii) The plastic zone evolves and propagates by a degradation law describing the softening of the rock expressed by the porosity dependent cohesion C and friction angle Φ. In this work we adopt two different laws as will be explained below. (iii) The dynamics of the mean porosity is deduced from the hydrodynamic erosion model of Vardoulakis et al.,[25] Papamichos et al[21] and Gravanis et al[8]

The experimental sample considered is a hollow cylinder with an inner and outer radius r_{in} and r_{out} respectively and with height H with a uniform radial stress σ_{out} applied at its external boundary. The external stress induces plastic yielding at a zone of thickness Λ, in the area of the inner radius as showed in Fig. 1. A radially uniform and constant flow rate Q is maintained throughout the duration of the test.

Following the works of Papamichos et al[21] and Gravanis et al[8] we assume that erosion will only occur within the plastic region. Although sanding may not be directly related to yielding of the rock, but rather related to the magnitude of strain, as mentioned in the introduction, we shall adopt the assumption explained above for simplicity. Fig. 2 shows a cross section of the hollow cylinder test sample where it focuses at the interface area where the plastic region Λ with mean porosity $\bar{\phi}$ meets the non-yielded elastic region with uniform (initial) ϕ_0 at time t. As the erosion process advances, plastic yielding evolves uniformly in all directions. At time $t + dt$ the plastic zone will have a thickness $\Lambda+d\Lambda$ and a mean porosity $\bar{\phi} + d\bar{\phi}$.

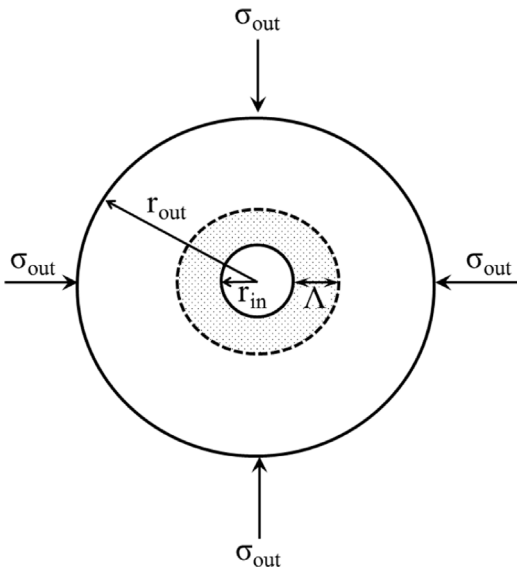

Fig. 1. Schematic representation of the hollow cylinder test.

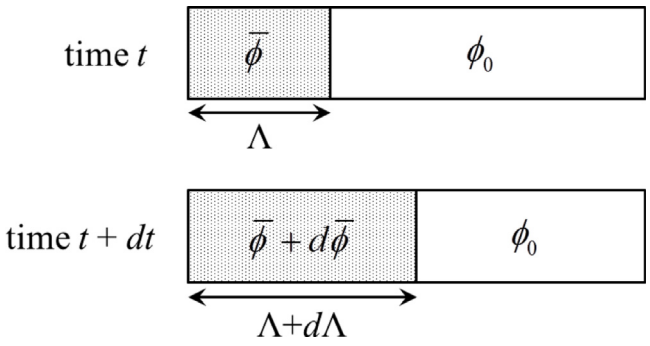

Fig. 2. Cross section of the sample (not to scale).

The specific form of the porosity field (e.g the Kozeny-Karman equation) is not important in our formulation. The mean porosity $\bar{\phi}$ within the plastic region and its thickness Λ will be the basic dynamical variables in our approach. The proposed semi-analytical model takes advantage of the hollow cylinder assuming axisymmetric conditions and has three components: (i) an elasto-plastic function of the material (e.g Mohr–Coulomb), (ii) a constitutive law for the degradation of the material (causing erosion), and (iii) a hydro-dynamic law for the erosion process (made possible by plastic yielding).

The governing equations of the model can be described as follows. In axisymmetric conditions, the stress field equation in the elastic region $r > R = r_{in} + \Lambda$ imply that, after neglecting the pressure dependent terms, yields[8]:

$$\sigma_r = \sigma_{out} + C_2 \left[\frac{1}{r_{out}^2} - \frac{1}{r^2} \right] \tag{1}$$

$$\sigma_\theta = \sigma_{out} + C_2 \left[\frac{1}{r_{out}^2} + \frac{1}{r^2} \right] \tag{2}$$

where σ_r, σ_θ are the radial and tangential components of the stress field and C_2 is an integration constant. In the plastic region $r < R = r_{in} + \Lambda$ the stress field is given by:

$$\sigma_r = -\frac{S_0}{k-1} \left[1 - \frac{r^{k-1}}{r_{in}^{k-1}} \right] \tag{3}$$

where S_0 is the uniaxial compressive strength, and the parameter k are given in terms of the cohesion C and friction angle Φ by equations:

$$k = \tan^2\left(\frac{\pi}{4} + \frac{\Phi}{2}\right), \qquad S_0 = 2C\sqrt{k} \tag{4}$$

The tangential component of the stress is given through the Coulomb failure criterion:

$$\sigma_\theta = S_0 + k\sigma_r \tag{5}$$

Given these equations, the plastic zone boundary which occurs at a radius $r = R$ is determined by the *continuity of the stress field* according to:

$$\sigma_{\theta\,\text{elastic}}(R) = \sigma_{\theta\,\text{plastic}}(R), \qquad \sigma_{r\,\text{elastic}}(R) = \sigma_{r\,\text{plastic}}(R) \tag{6}$$

One of these equations fixes the constant C_2 and the other one provides the equilibrium constraint which defines R in terms of the material parameter and the boundary conditions.

The equilibrium constraint takes the form of a surface in the space of the variables R, C, Φ, σ_{out} defined by

$$F(R, C, \Phi, \sigma_{\text{out}}) = 0 \tag{7}$$

where

$$F(R, C, \Phi, \sigma_{\text{out}}) = (k-1)S_0 r_{\text{in}} R^{k+1} + (k+1)S_0 r_{\text{out}}^2 r_{\text{in}} R^{k-1} - 2(S_0 + (k-1)\sigma_{\text{out}})r_{\text{out}}^2 r_{\text{in}}^k \tag{8}$$

Changing the values of C and Φ by degradation and, in general, varying also σ_{out}, moves R along that surface according to

$$dF = \frac{\partial F}{\partial R}dR + \frac{\partial F}{\partial C}dC + \frac{\partial F}{\partial \Phi}d\Phi + \frac{\partial F}{\partial \sigma_{\text{out}}}d\sigma_{\text{out}} = 0 \tag{9}$$

where the derivatives in this expression amount to cumbersome expressions which we shall refrain from writing down explicitly. The formulation of the mechanics of the problem is now complete.

Degradation of the material is expressed by allowing the cohesion and friction angle to depend on porosity, which in our case is represented by the mean porosity:

$$C = C(\bar{\phi}), \quad \Phi = \Phi(\bar{\phi}) \tag{10}$$

For the time being, we shall keep that dependence general.

The hydro-dynamic erosion law is formulated building on the model of Vardoulakis et al[25] as elaborated by Papamichos et al.,[21] see also Ref. 8. We introduce the mean porosity within the plastic zone is defined by suitably integrating the porosity field:

$$\bar{\phi} = \frac{1}{\Lambda}\int_{r_{\text{in}}}^{R} \phi\, dr = \frac{1}{\Lambda}\int_{r_{\text{in}}}^{r_{\text{in}}+\Lambda} \phi\, dr \tag{11}$$

The constitutive equation of Vardoulakis et al[25] reads

$$\frac{\partial \phi}{\partial t} = \lambda f(\phi) q \tag{12}$$

where λ [m^{-1}] is the sand production coefficient which is assumed constant, q is the Darcy flux of the fluid, and f is a function of porosity, which in the previous formulations was taken to be $f(\phi) = 1 - \phi$, although it may take quite different forms, as long as $f(1) = 0$, which enforces that porosity will stop increasing at the value 1. We shall not consider the effects of critical drawdown, which can be included in this equation by substituting the Darcy flux q with q–q_{cr} where q_{cr} is a constant realizing critical drawdown,[3,35] as it can be easily included in the equations of the proposed framework. Continuity implies that the radial Darcy flux q reads[8]:

$$q = \frac{Q}{2\pi H r} \tag{13}$$

From Eq. (11), the time-variation of the mean porosity take the form (see Appendix A)

$$d\bar{\phi} = -\frac{d\Lambda}{\Lambda}\bar{\phi} + \frac{d\Lambda}{\Lambda}\phi_0 + dt\,\frac{1}{\Lambda}\int_{r_{in}}^{R}\frac{\partial \phi}{\partial t}dr \tag{14}$$

Using now the hydrodynamic erosion Eq. (12) and approximating suitably the integral, we obtain

$$d\bar{\phi} \simeq \frac{d\Lambda}{\Lambda}(\phi_0 - \bar{\phi}) + \frac{\lambda Q}{2\pi H(r_{\text{in}} + \gamma\Lambda)}f(\bar{\phi})dt \tag{15}$$

where the constant γ ($0 < \gamma < 1$) is a parameter that depends on the (unknown and irrelevant in the present formulation) profile of the porosity field; the constant γ arises by roughly approximating the integral $\Lambda^{-1}\int f(\phi)r^{-1}dr \approx (r_{\text{in}} + \gamma\Lambda)^{-1}f(\bar{\phi})$ which arises when substituting Eqs. (12) and (13) into Eq. (14). The parameter γ can be obtained self-consistently as we explain below. It should be emphasized that Eq. (15) can be regarded as the defining equation for the time evolution of the mean porosity in the presented framework.

Eqs. (9) and (10) imply a relation between the increments of the plastic zone radius R (and hence of the plastic zone depth Λ) and the mean porosity:

$$d\Lambda = dR = -F_\phi\, d\bar{\phi} - F_\sigma\, d\sigma_{\text{out}} \tag{16}$$

where

$$F_\phi = \frac{\frac{\partial F}{\partial C}C' + \frac{\partial F}{\partial \Phi}\Phi'}{\frac{\partial F}{\partial R}}, \quad F_\sigma = \frac{\frac{\partial F}{\partial \sigma_{\text{out}}}}{\frac{\partial F}{\partial R}} \tag{17}$$

where prime denotes differentiation with respect to mean porosity. Combining Eqs. (16) with Eq. (15) we obtain an evolution equation for the plastic zone depth:

$$d\Lambda = u\, dt \tag{18}$$

where u is the speed of advancement of the plastic yielding, and it is defined by

$$u = -\frac{F_\phi}{1 + \frac{(\phi_0 - \bar{\phi})}{\Lambda}F_\phi} \times \left[\frac{\lambda Q}{2\pi H(r_{\text{in}} + \gamma\Lambda)}f(\bar{\phi}) - \frac{(\phi_0 - \bar{\phi})}{\Lambda}F_\sigma\frac{d\sigma_{\text{out}}}{dt}\right] - F_\sigma\frac{d\sigma_{\text{out}}}{dt} \tag{19}$$

Eqs. (16) and (19) imply that the mean porosity varies with time according to

$$d\bar{\phi} = \frac{1}{1 + \frac{(\phi_0 - \bar{\phi})}{\Lambda}F_\phi} \times \left[\frac{\lambda Q}{2\pi H(r_{\text{in}} + \gamma\Lambda)}f(\bar{\phi})dt - \frac{(\phi_0 - \bar{\phi})}{\Lambda}F_\sigma d\sigma_{\text{out}}\right] \tag{20}$$

Note that, due to radial symmetry, σ_{out} may be a function of time or a pure constant. In the latter case, all terms proportional to $d\sigma_{\text{out}}$ vanish. Hence, we have a system of two ordinary differential equations governing explicitly the evolution of the plastic zone depth and mean porosity. They can be regarded as the defining equations of the proposed model, which may be regarded as a kinematic formulation of the hydro-mechanical description of the erosion process. The produced mass can be then derived along the lines of Gravanis et al[8] to obtain

$$dM = dt\,\rho_s 2\pi H\,\lambda\int_{r_{\text{in}}}^{r_{\text{in}}+\Lambda} f(\phi)\frac{Q}{2\pi H r}r dr \simeq \rho_s\lambda\Lambda f(\bar{\phi})Q dt \tag{21}$$

where ρ_s is the mass density of the rock, where in the last equality we simplify the integral by its first approximation in terms of the mean porosity. The parameter γ, introduced in Eq. (15) is determined self-consistently so that the eroded mass at late times

to be equal with the mass of the sample. This completes the formulation of the framework.

The general analysis of the model can be clarified by introducing suitable scales for the various variables in order to work with dimensionless quantities. Inspecting Eq. (15) and in particular the second term, we may introduce the following time scale for the erosion phenomenon:

$$\frac{1}{T} = \frac{\lambda Q}{2\pi(r_{\text{out}} - r_{\text{in}})H} \tag{22}$$

Additionally, a speed scale reads

$$U = \frac{r_{\text{out}} - r_{\text{in}}}{T} = \frac{\lambda Q}{2\pi H} \tag{23}$$

We may now specify the hydro-dynamical erosion and degradation models. The hydro-dynamic Eq. (12) takes the specific form assuming that the function f reads

$$f(\overline{\phi}) = \left(\frac{\overline{\phi}}{\phi_0}\right)^{a_H}(1-\overline{\phi}) \tag{24}$$

for some constant exponent a_H whose effect will be investigated in what follows. This function has the necessary property $f(1) = 0$ but also has the property that vanishes for low porosity values.

The degradation models which are considered take the form

$$C(\overline{\phi}) = C_0\left(\frac{1-\overline{\phi}}{1-\phi_0}\right)^{a_D} \tag{25}$$

$$\Phi(\overline{\phi}) = \Phi_0\left(\frac{1-\overline{\phi}}{1-\phi_0}\right)^{a_D} \tag{26}$$

where C_0, Φ_0, are the initial values of the cohesion and friction angle respectively. The exponent a_D quantifies a non-linear dependence of the cohesion/friction angle, effectively degradation becomes stronger at lower values of the porosity, and the exponent a_H quantifies a (power-law) dependence of the erosion rate in the lower porosity regime.

For completeness, we write down the initial value of the mass of the sample,

$$M_{\text{sample}} = (1-\phi_0)\rho_s\pi(r_{\text{out}}^2 - r_{\text{in}}^2)H \tag{27}$$

to be used in scaling the sand production mass in the next section.

3. Analysis and results

Following the formulation of the proposed model in the previous section, we now turn our focus to the analysis of the model parameters. We begin our discussion when applying the simplified model in the case of the experiment of Papamichos et al[21] Given that the sand production coefficient λ is not known, the only way to test the model is to estimate its values for the different values of external stress considered in the experiment of Papamichos et al[21] as well as to compare the predicted sand production curves with the new semi-analytical model against the experimental ones. As it was shown in Ref. 8 the effect of changing the flow rate amounts essentially to a rescaling of time in these models, hence the external stress is left as the non-trivial factor of influence. We shall use λ as the single fitting parameter for these estimations, as opposed to the back analysis procedures employed in Refs. 8, 16 where three-parameter best fit was used. Preliminary work in this model was presented in Ref. 37.

3.1. Parametric analysis of degradation laws and hydro-dynamic constitutive equations

The geometric properties of the hollow cylinder sample and the mechanical properties of the rock are summarized in Table 1.

Table 1
Model properties and input data.

Variable	Value
Geometric properties	
Hollow cylinder internal radius, r_{in} [m]	0.01
Hollow cylinder external radius, r_{out} [m]	0.1
Cylinder height, H [m]	0.2
Rock properties	
Initial cohesion, C_0 [MPa]	3.7
Initial friction angle, Φ_0 [°]	37.4
Initial porosity, ϕ_0 [–]	0.3
Mass density, ρ_s [kg/m^3]	2640
Model parameters	
Degradation control parameter, a_D [–]	{1, 1.5, 2, 3}
Hydro-dynamic control parameter, a_H [–]	{0, 3}

The necessary physical parameters were taken from Ref. 21. The values of the external stress used in that experiment were $\sigma_{\text{out}} = \{7.5, 8, 9, 10, 11\}$ MPa, and with a flow rate $Q = 0.5$ L/min, which corresponds to a drawdown pressure equal with 0.15 MPa and was considered constant throughout the experiment. The elastic properties of the material affect only the pressure dependent terms in the equation determining the plastic zone thickness Λ,[8] hence they are irrelevant in the present formulation. We proceed to analyze the influence of different degradation rates as defined by Eqs. (25) and (26) and different hydrodynamic erosion constitutive equations defined by Eq. (24).

Fig. 3 presents the behavior of the friction angle and cohesion as a function of the porosity. It is noted that the initial porosity considered begins from 0.3. The parameter a_D that expresses the rate of softening, controls how fast friction angle and cohesion become practically zero. For example, if one considers the largest value of a_D, friction angle and cohesion practically vanish for porosity 0.8.

In Fig. 4, we present the influence of the degradation control parameter expressing the softening rate a_D on the evolution of sand production, porosity, plastic zone depth and plastic yielding speed in terms of dimensionless time using the scale in Eq. (22). This analysis is for the case of hydrodynamic control parameter $a_H = 0$. Specifically, sand production is expressed in terms of dimensionless ratio of eroded mass/sample mass and the plastic yielding speed is expressed in the dimensionless form divided by the scale U defined in Eq. (23). The plastic zone is given in dimensionful form following the sample size of the experiment of Papamichos et al[21] The sensitivity analysis was performed for the data presented in Table 1 and for a given external stress of 11 MPa and a flow rate of 0.5 L/s. Fig. 4a shows that the non-linear degradation law exhibits a qualitative difference from the linear law ($a_D = 1$) although all cases converge smoothly to mass ratio value 1.0. The evolution of porosity in Fig. 4b exhibits two regimes: initially, plastic yielding is advancing while the erosion process operates on the material within the plastic zone, and in the second regime, it appears that the plastic zone (yielding) has already reached the outer boundary of the rock and hence erosion process is active in the entire rock sample. We observe that as the rate of softening a_D increases, plastic yielding reaches the outer boundary faster, while the mean porosity initially is smaller for larger values of the softening rate, which is a mere implication of the larger plastic zone that has been created. Fig. 4c shows the explicit evolution of the plastic zone depth Λ as plastic yielding traverses, the radial size of the sample (r_{out}–$r_{\text{in}} = 0.09$ m). Fig. 4d presents the speed of plastic yielding, that is, the slope of the curves in Fig. 4c, in dimensionless form. One observes that the speed increases with the softening rate, starting from a nearly constant speed for the linear degradation law ($a_D = 1$) to a faster

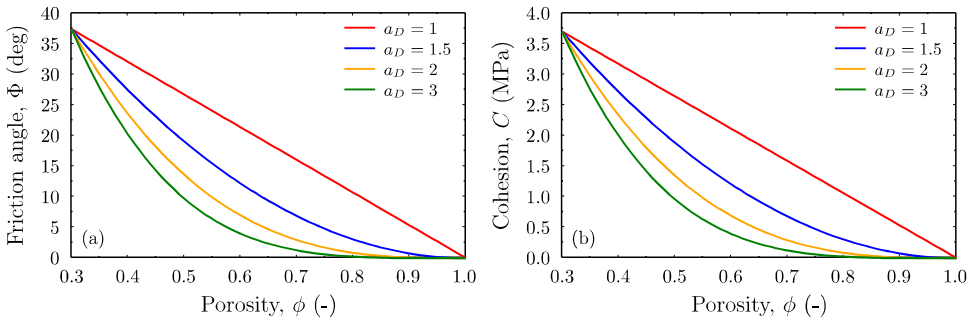

Fig. 3. Degradation of friction angle and cohesion according to Eqs. (25), (26).

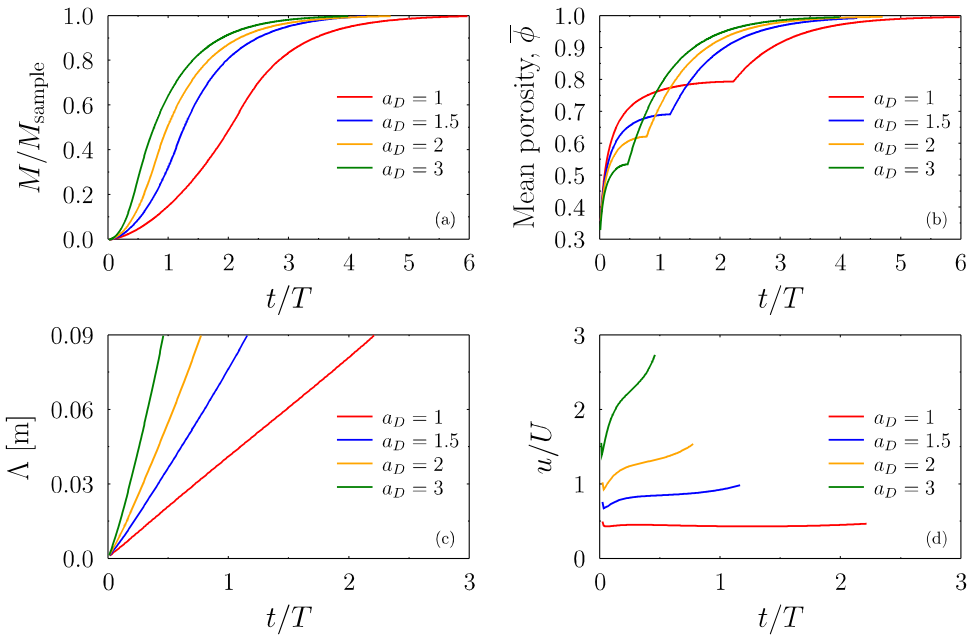

Fig. 4. Influence of rate of softening (a_D) for exponent $a_H = 0$ (constitutive Eq. (24)).

and continuously accelerating yielding as a_D increases. We should note that the case considered in Fig. 4a–d which refers to the hydrodynamic exponent $a_H = 0$ and for the linear degradation law $a_D = 1$ (red-line curves) corresponds to the usual forms of the constitutive (hydrodynamic) and degradation laws used in Refs. 8, 20, 21.

We now present the case of hydrodynamic exponent $a_H = 3$ of Eq. (24) as it is analyzed in Fig. 5 for the same physical variables as in the previous case ($a_H = 0$). (The analysis performed for this case also, utilized the data of Table 1 for external stress 11 MPa and a flow rate of 0.5 L/s.) In Fig. 5a we observe again that the non-linear degradation laws differ qualitatively from the linear one and in fact in this case the considered value for the softening rate leads to a collapse of all sand production curves. We also observe that the rate of sand production becomes much more rapid as compared to the previous case of $a_H = 0$. This is evident from the much less times it takes to erode away the entire sample. That is, the modification of the hydrodynamic law in the low porosity regime accelerates the erosion process and hence, through degradation, the rate of plastic yielding. This is clarified mathematically in Appendix B. Fig. 5b shows that the change of regime occurs within a relatively short interval i.e., the time that plastic yielding reaches the outer boundary of the sample does not differ significantly. Interestingly, for the case considered $a_H = 3$, the porosity curves almost coincide in the second regime.

The kinematics of the plastic yielding advancement is presented in Fig. 5c and d. Plastic yielding progresses in an accelerating fashion which increases for a higher values of the softening rate a_D, while the speed of advancement attains much higher values as compared to the previous case examined, $a_H = 0$. (It should be noted that negative values of the exponent a_H lead to a concave rather than convex mass production curves, as it can be observed in Fig. 4a and 5a, in the early stages. This behavior is phenomenologically inconsistent with the experimental data shown in Fig. 6 in the next section. For this reason we shall consider only the case $a_H \geq 0$.

3.2. Comparison with the hollow cylinder experiment of Papamichos et al[21]

In the next step of our analysis, we present an application of the proposed framework utilizing the hydrodynamic and degradation constitutive expressions given in Eqs. (24)–(26) to compare the theoretically predicted sand production curves of the semi-analytical model with the experimental data of Papamichos et al[21] We consider four test cases: for each of the linear ($a_D = 1$) and non-linear ($a_D = 3$) degradations we investigate the cases $a_H = 0$ and $a_H = 3$ of the hydrodynamic law. These values correspond to the extreme values of these exponents analyzed in Section 3.1.

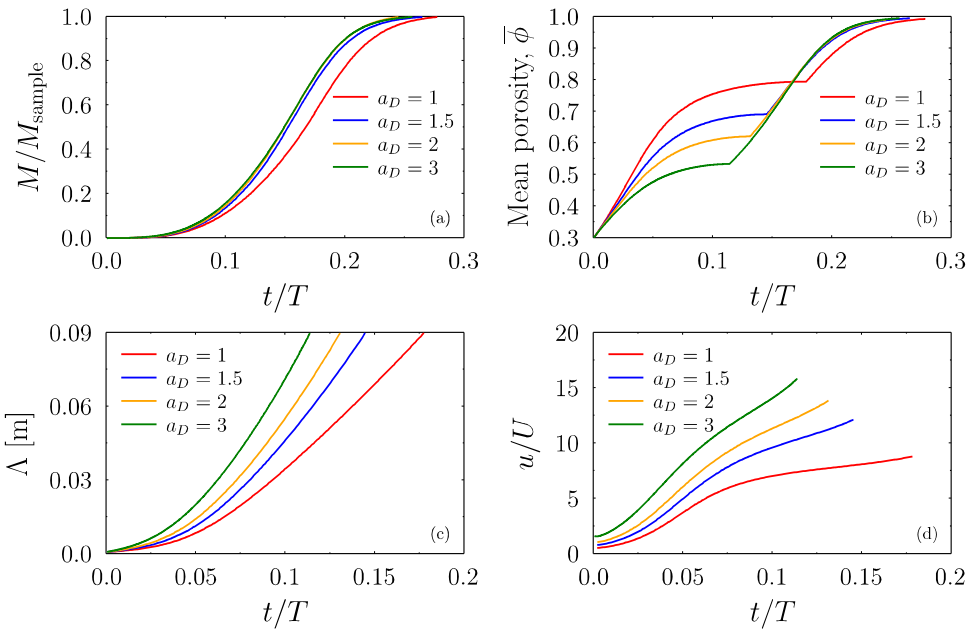

Fig. 5. Influence of rate of softening (a_D) for exponent $a_H = 3$ (constitutive Eq. (24)).

In Fig. 6a–e we present the theoretical sand production curves for the four cases mentioned above compared against the experimental data presented in Ref. 21. Also, Fig. 6f shows the estimated values of the sand production coefficient λ (with units m^{-1}) as obtained from best fitting the theoretical curves produced with the proposed semi-analytical model with the experimental data solving for the four cases and for each stress level. The sanding data of Papamichos et al[21] are depicted with circle markers, while the theoretical sand production curves are shown as follows: red color corresponds to $a_H = 0$ and blue color to $a_H = 3$; dashed lines indicate $a_D = 1$ and continuous lines to $a_D = 3$.

This analysis presents the behavior of the considered hydrodynamic and degradation laws against the experimental data for various external stresses. As expected, differences between the theoretically predicted sand production curves and the experimental data are observed. In particular, the late stage of the experimental sand production is not followed properly. The observed reduction of the erosion rate may be explained by the yielded zone accepting that in the late stage the rock has eroded away to a great extent. Such picture is qualitatively consistent with our conceptual description of the process as an interplay between the speed of yielding and erosion advancement, although quantitatively the simple hydrodynamic and degradation laws we employed are not effective quantitatively. To our knowledge no existing model captures that behavior properly. Also, the data may have been affected by the gradual change of the external stress in the experiment of Papamichos et al[21] The proposed semi-analytical framework based on two ODE's may be effectively and efficiently used to check and calibrate much more refined hydrodynamic and degradation laws which could describe actual data with greater accuracy. It also may be of interest to note that the values of the sand production coefficient λ follow a certain pattern for all test cases We also observe that the variability of λ with the stress is weakened as the non-linearity is intensified in the degradation and the low porosity regime of the hydrodynamic laws.

Fig. 7a and b show the solution of the semi-analytical model for the simplest case of hydrodynamic and degradation laws corresponding to the parameters $a_H = 0$ and $a_D = 1$. The solution involves the two basic variables of the kinematic formulation of the erosion process i.e the evolution of the mean porosity (Fig. 7a) and the plastic zone (Fig. 7b) as a function of the external stress. The simplest case of $a_H = 0$ and $a_D = 1$ corresponds to the constitutive laws used originally by Vardoulakis et al[25] The solution for the other cases of hydrodynamic and degradation laws parameters is qualitatively similar to the behavior observed in Fig. 7.

Table 2
Best fit parameters α, β of the Eq. (28).

a_H [–]	a_D [–]	α [m^{-1}]	β [–]
0	1	0.111	1.598
3	1	0.070	1.446
0	3	0.065	1.124
3	3	0.048	1.041

It may be observed that the evolution of the mean porosity, does not exhibit an obvious trend with respect to the external stress primarily due to the effect of the calibrated sand production coefficient. Overall, the mean porosity predicted is not radically different for the various values of external stress considered. On the other hand, the plastic zone depth is consistently larger with the increase of the externally applied stresses, as expected. One may note that for the smallest applied stress (7.5 MPa), which is close to the no-yielding limit (7.41 MPa), the plastic zone depth exhibits a very significant change relatively to its initial value. This is due to the significant role played by erosion and degradation of the material in this case.

In our previous work[19] we proposed a power law dependence of the sand production coefficient λ on the external stress, under the assumption that λ is zero at the minimum stress for yielding (7.41 MPa). In this work, we propose a modified power law dependence with decreasing exponential factor:

$$\lambda(\sigma) = \alpha \left(\frac{\sigma - \sigma_{\min}}{\sigma_{\min}} \right)^{1/6} \exp\left[-\beta \left(\frac{\sigma - \sigma_{\min}}{\sigma_{\min}} \right) \right] \tag{28}$$

where α [m^{-1}], β [–] are constants to be determined by best fit, $\sigma_{\min} = 7.41$ MPa and the power law exponent is taken from Ref. 19. Constants α and β after best fit determination are presented in Table 2.

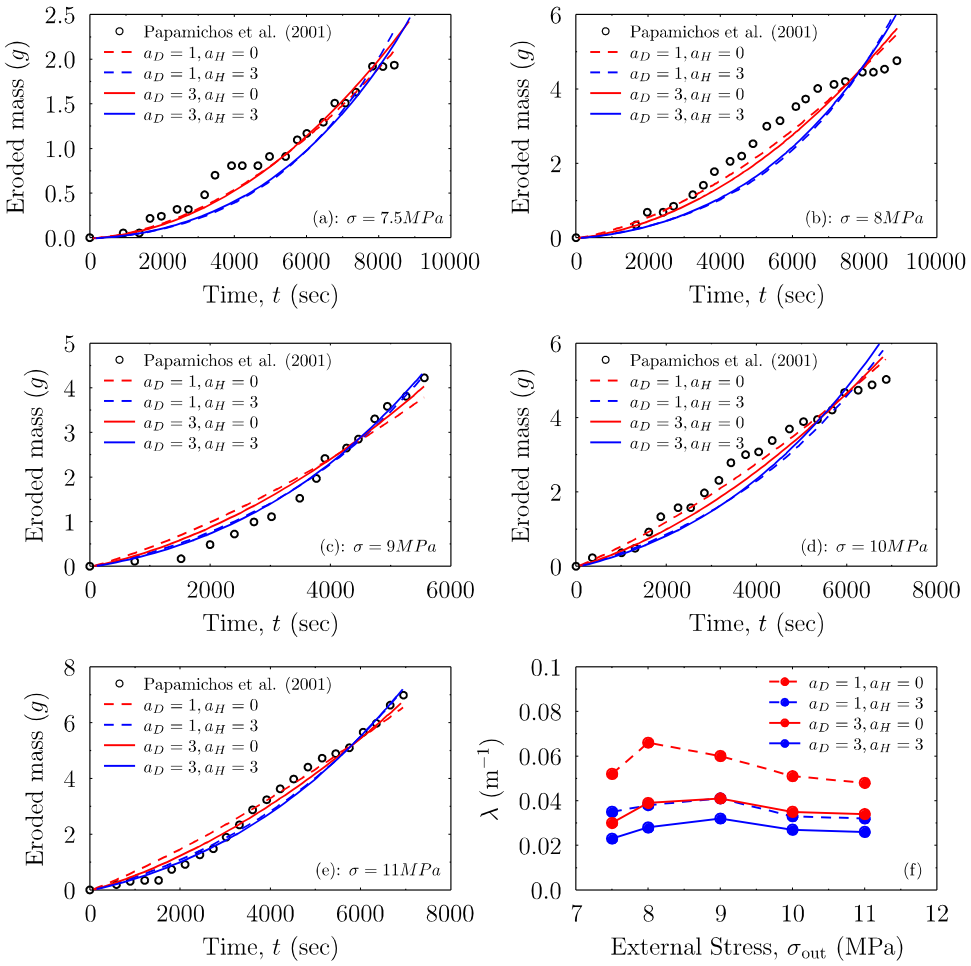

Fig. 6. Comparison of the test cases of the degradation and hydrodynamic laws (Eqs. (24)–(26)) against the experiments of Papamichos et al[21] Red color corresponds to $a_H = 0$ and blue color to $a_H = 3$; dashed lines indicate $a_D = 1$ and continuous lines to $a_D = 3$.

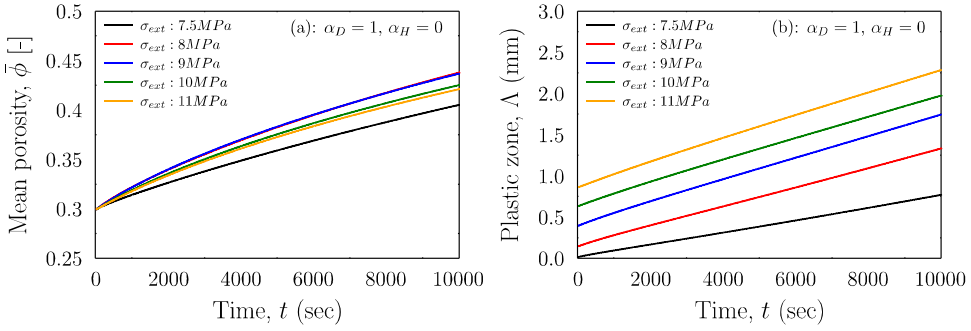

Fig. 7. Mean porosity and plastic zone evolution for different external stresses.

For the values of the parameters α, β presented in Table 2 corresponding to the different cases of hydrodynamic and degradation laws we plot Eq. (28) in Fig. 8 together with the values of λ obtained previously and shown in Fig. 6f. It should be noted that the values of the parameters α, β are material dependent.

3.3. Comparison with the experiment of Kooijman et al[38]

This experiment presented in Ref. 38, see also Ref. 14 was performed on artificial sandstone block which according to rock mechanics is characterized as a weak rock with dimensions 26.25 cm $\times$ 26.25 cm $\times$ 38 cm. The sandstone block has a central horizontal hole of 25.4 mm diameter which is aligned with the longer axis of the sample. To compute the erosion process, they applied a far-field stress on the surfaces of the sample with a ratio of effective stresses vertical/horizontal equal with $\sigma_v/\sigma_h = 2$. The stresses varied continuously during the sanding test according to Fig. 9a where the vertical stress is depicted. Also, the flow rate was varied during the test as shown in Fig. 9b corresponding to a maximum drawdown pressure of 25 psi equal to 0.17 MPa.[38] The relevant parameters to our semi-analytical model concerning the artificial block sample used in the sanding experiments of Kooijman et al[38] and Van den Hoek et al[14] are summarized in Table 3.

In the context of our formulation, we approximate the conditions of the experiment as follows. The geometry of the artificial

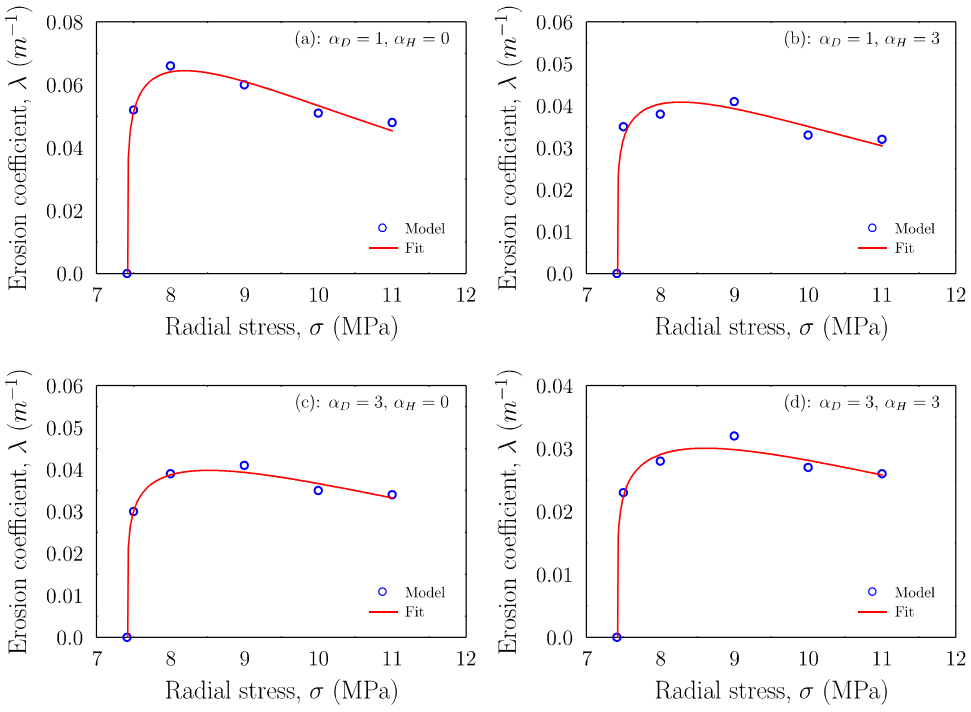

Fig. 8. Best fit of Eq. (28) for the four cases of the degradation and hydrodynamic laws.

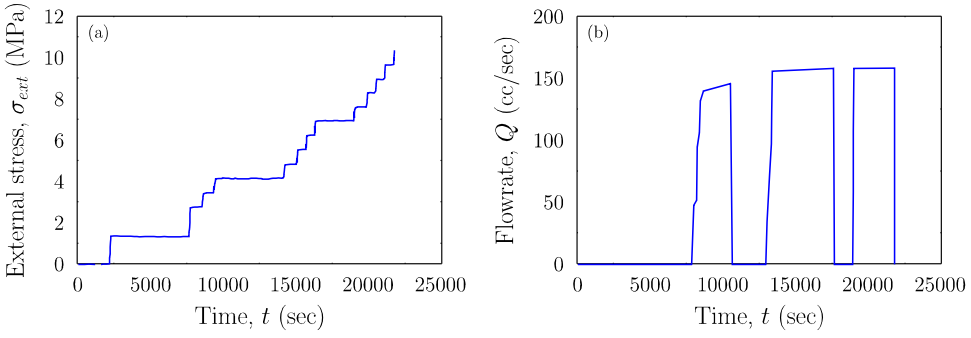

Fig. 9. Input data of (a) external stress and (b) flowrate for modeling the sanding experiment of Kooijman et al[38]

Table 3
Relevant parameters of the experiment of Kooijman et al[38].

Variable	Value
Artificial sample properties	
Initial cohesion, C_0 [MPa]	1.25
Initial friction angle, Φ_0 [°]	37.5
Initial porosity, ϕ_0 [–]	0.34
Mass density, ρ_s [kg/m^3]	1750
Model parameters	
Degradation control parameter, a_D [–]	1
Hydro-dynamic control parameter, a_H [–]	0
Sand production coefficient, λ [m^{-1}]	0.020

sample is approximated as a cylinder of outer radius $r_{\text{out}} = 26.25/2$ cm $= 13.125$ cm. The external stress σ_{out} is approximated as isotropic and equal to σ_{v} of the experimental test of Kooijman et al.,[38] with its time variation given in Fig. 9a. Approximating σ_{out} this way it is necessary for the initiation of sand production as deduced by the model to be consistent with the experimental data. In particular, for the given artificial sample the minimum external stress to initiate material plastic yielding turns out to be 2.58 MPa which is entirely consistent with erosion onset in this sanding experiment as it will be discussed below.

Fig. 10 shows the predicted sand production mass curve (gr) by the semi-analytical model for a constant sand production coefficient $\lambda = 0.020$ m^{-1} (see Table 3) and using the simplest hydrodynamic and degradation laws corresponding to the parameters $a_H = 0$ and $a_D = 1$. The sand production coefficient is calibrated as a constant, that is, independent of the external stress, for simplicity. The calibration of predefined model $\lambda(\sigma)$ such as the one given in Eq. (28) will be performed in future work. It can be observed that the predicted sand production curve (red continuous line) is in good agreement with the experimental one (blue continuous line).

A qualitative difference between the curves is that the experimental sand production remains flat between 13k to 15k seconds while the flow rate is not zero in this time interval. The reason for this behavior possibly is the non-continuous nature of the actual erosion process. It should be emphasized that both curves indicate a simultaneous on-set of sand production which is consistent with our model assumption that erosion is directly linked with plastic yielding. Onset of sanding in the experiment occurs when $\sigma_{\text{v}} \sim 2.6$ MPa. As mentioned above, this is consistent

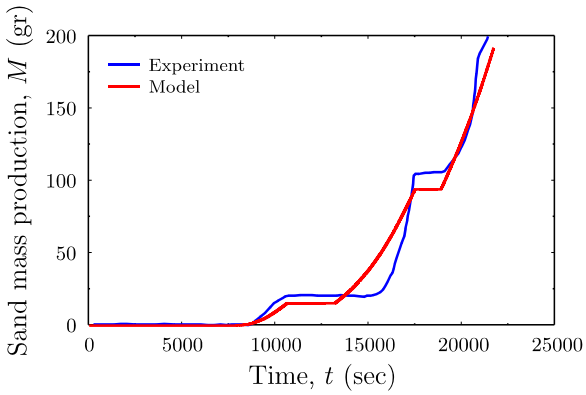

Fig. 10. Comparison between the proposed semi-analytical model and the experimental data of Kooijman et al[38] (see also Ref. 14).

with initiation of plastic yielding in the context of our modeling of the experiment.

Fig. 11 presents the evolution with time of the basic variables, mean porosity and plastic zone depth, according to our modeling of the Kooijman et al[38] experiment. According to the solution of our model, we observe that during intervals of erosion advancement, alternate with intervals during which erosion stops. In particular, the mean porosity stops evolving when flow rate vanishes while the plastic zone depth evolution halts when also the external stress remains constant (see also Fig. 9a, b). The trend of both variables is clearly affected by the increase of the externally applied stress.

4. Summary and conclusions

In this work we introduce a novel semi-analytical hydro-mechanical framework for modeling sanding in the context of the hollow cylinder test, aiming at providing an effective tool for studying the influence of the hydrodynamic and material degradation constitutive laws, and calibrating the sand production coefficient. In spite of the fact that hydromechanical modeling of erosion exists for quite some time, a detailed phenomenological analysis of its performance is still lacking. This presents a certain deficit in the literature given that the detailed physical mechanisms of the erosion process are not transparently known.

The theoretical premise adopted in this work is that erosion occurs within the plastic zone controlled by a hydrodynamic constitutive law. In the hydro-mechanical modeling of erosion, advancement of the plasticity zone is treated quasi-statically and it is coupled with the hydrodynamic erosion law by material degradation. The developed plastic zones are created according to Mohr–Coulomb criterion. The radial symmetry of the hollow cylinder test reduces the problem to one spatial dimension.

In the proposed modeling we introduce a number of simplifications are employed. (1) The direct effects of plastic strains on the development of the erosion process are neglected. (2) As a practical simplification we restrict ourselves to cases where the pressure drawdown is essentially negligible with respect to the applied stresses. (3) We model the *mean value* of the porosity field within the plastic zone and use it as a basic variable. The degradation and hydrodynamic laws are expressed in terms of this variable. Hence, we arrive at a *kinematic description* of the erosion process, expressed by two coupled ODEs governing the mean porosity and the radial depth of the plastic zone. The latter variable is governed by quasi-static equilibrium. The simplicity of the obtained framework greatly facilitates the analysis of the effect of different hydrodynamic and degradation laws, the calibration of the sand production coefficient, and a quick estimation of sand production curves.

In the context of this formulation, we study the influence of different forms of hydrodynamic laws, modified in the low porosity regime, and the degradation law, considering non-linear dependence of cohesion and friction angle on the mean porosity. We find quantitative but not major qualitative effects on the sand production induced by the different laws. Additionally, we set the obtained models against two different sanding experimental tests, Papamichos et al[21] and Kooijman et al[38] We find good agreement with the measured sand production curves. The test of Papamichos et al[21] is used to calibrate a modeled dependence $\lambda(\sigma)$ of the sand production coefficient λ on the external stress, a power law modified by a decreasing exponential factor. A power law model $\lambda(\sigma)$ was introduced in a previous work of the authors using numerical modeling of the erosion.

The proposed framework can be further elaborated to include the effects of pressure as well as the effects of plastic strain in a semi-analytic fashion. These inclusions will expand the kinematic formulation so that to refine the physics of the erosion it implements and widen the range of its applications in experimental tests and field applications where drawdown pressure is not negligible compared to the applied stress. These research endeavors will be presented in future work.

CRediT authorship contribution statement

Panayiotis Kakonitis: Conceptualization, Methodology, Software creation, Validation of results, Writing – original draft, Visualization-graphics, Writing – review & editing. **Elias Gravanis:** Conceptualization, Methodology, Software creation, Validation of results, Writing – original draft, Visualization-graphics, Writing – review & editing. **Ernestos N. Sarris:** Conceptualization, Methodology, Software creation, Validation of results, Writing – original draft, Visualization-graphics, Writing – review & editing.

Declaration of competing interest

The authors declare that they have no known competing financial interests or personal relationships that could have appeared to influence the work reported in this paper.

Data availability

No data was used for the research described in the article.

Appendix A

Differentiating Eq. (11) with respect to time we obtain

$$\begin{aligned}\frac{d\bar{\phi}}{dt} &= \frac{d}{dt}\left(\frac{1}{\Lambda}\int_{r_{\text{in}}}^{r_{\text{in}}+\Lambda}\phi\, dr\right) = -\frac{1}{\Lambda^2}\frac{d\Lambda}{dt}\int_{r_{\text{in}}}^{r_{\text{in}}+\Lambda}\phi\, dr \\ &\quad + \frac{1}{\Lambda}\phi(r=r_{\text{in}}+\Lambda)\frac{d\Lambda}{dt} + \frac{1}{\Lambda}\int_{r_{\text{in}}}^{r_{\text{in}}+\Lambda}\frac{\partial\phi}{\partial t}dr \\ &= -\frac{1}{\Lambda}\frac{d\Lambda}{dt}\bar{\phi} + \frac{1}{\Lambda}\phi_0\frac{d\Lambda}{dt} + \frac{1}{\Lambda}\int_{r_{\text{in}}}^{r_{\text{in}}+\Lambda}\frac{\partial\phi}{\partial t}dr\end{aligned} \tag{A.1}$$

where we used the Leibniz rule for differentiating the integral (with time dependent end-points),

$$\begin{aligned}\frac{d}{dt}\int_{r_1(t)}^{r_2(t)} f(r,t)dr &= f(r_2(t),t)\frac{dr_2(t)}{dt} - f(r_1(t),t)\frac{dr_1(t)}{dt} \\ &\quad + \int_{r_1(t)}^{r_2(t)}\frac{\partial f(r,t)}{\partial t}dr\end{aligned} \tag{A.2}$$

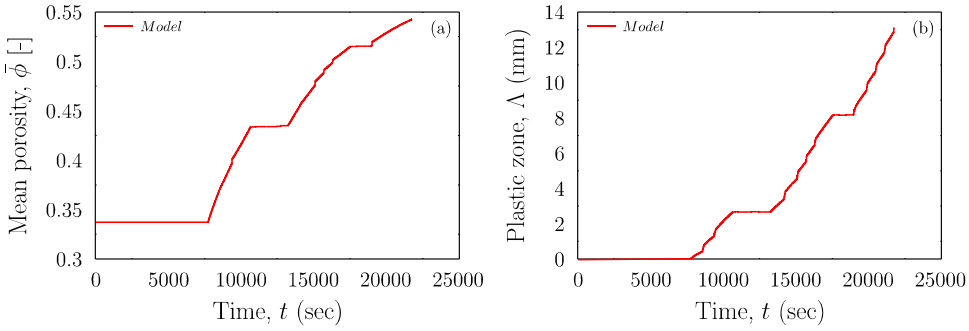

Fig. 11. Mean porosity and plastic zone evolution for the experimental test of Kooijman et al[38] (see also Ref. 14).

for integrating a time-dependent function f between moving endpoints r_1 and r_2. We also used the fact $\phi = \phi_0$ at $r = R = r_{\text{in}} + \Lambda$, and employed Eq. (11) in the first term of (A.1). Hence, we arrive at Eq. (14) of the main text:

$$d\bar{\phi} = -\frac{d\Lambda}{\Lambda}\bar{\phi} + \frac{d\Lambda}{\Lambda}\phi_0 + dt\frac{1}{\Lambda}\int_{r_{\text{in}}}^{r_{\text{in}}+\Lambda}\frac{\partial\phi}{\partial t}dr \tag{A.3}$$

Appendix B

In the low porosity regime, the hydrodynamic law given in Eq. (24) takes the form

$$\frac{\partial\phi}{\partial t} = \left(\frac{\phi}{\phi_0}\right)^{a_H} \tag{B.1}$$

This approximation holds for early times, and it is more accurate for small initial porosity. For $a_H \geq 1$, this is integrated to give

$$a_H = 1 \quad : \quad \phi = \phi_0 \exp\left(\frac{t}{\phi_0}\right) \tag{B.2}$$

$$a_H > 1 \quad : \quad \phi = \phi_0\left(1 - \frac{a_H - 1}{\phi_0}t\right)^{-\frac{1}{a_H - 1}} \tag{B.3}$$

The range $a_H \geq 1$ covers the case $a_H = 3$ presented in Fig. 5. From the formulas (B.2) and (B.3) we observe for these cases the porosity increases rapidly in the early stages of the phenomenon, hence explaining the acceleration of the erosion process for $a_H \geq 1$.

References

1. Qiu K, Marsden R, Alexander J, Retnanto A, Abdelkarim OA, Ben Shatwan MB. Practical approach to achieve accuracy in sanding prediction. In: *SPE Asia Pacific Oil & Gas Conference and Exhibition, Vol. 61*. OnePetro; 2006:130–140. conditions. International Journal of Rock Mechanics and Mining Sciences.
2. Osisanya SO. Practical guidelines for predicting sand production. In: *Nigeria Annual International Conference and Exhibition*. OnePetro; 2010.
3. Papamichos E. Analysis of borehole failure modes and pore pressure effects. *Comput Geotech*. 2010;37(1–2):141–152.
4. Rahmati H, Jafarpour M, Azadbakht S, Nouri A, Vaziri H, Chan D, Xiao Y. Review of sand production prediction models. *J Pet Eng*. 2013. http://dx.doi.org/10.1155/2013/864981.
5. Volonté G, Francesco S, Brignoli M. Sand prediction: a practical finite-element 3D approach for real field applications. *SPE Prod Oper*. 2013;28(01):95–108.
6. Ikporo B, Sylvester O. Effect of sand invasion on oil well production: a case study of Garon field in the Niger Delta. *Int J Eng Sci*. 2015;4(5):64–72.
7. Wang H, Sharma MM. A fully 3-D, multi-phase, poro-elasto-plastic model for sand production. In: *Proceedings of the SPE Annual Technical Conference and Exhibition*. OnePetro; 2016.
8. Gravanis E, Sarris E, Papanastasiou P. Hydro-mechanical erosion models for sand production. *Int J Numer Anal Methods Geomech*. 2015;18(39):2017–2036.
9. Gravanis E, Sarris E, Papanastasiou P. A hydro-mechanical erosion analytical model for sand prediction. In: *50th US Rock Mechanics/Geomechanics Symposium*. 2016.
10. Gholami R, Aadnoy B, Rasouli V, Fakhari N. An analytical model to predict the volume of sand during drilling and production. *J Rock Mech Geotech Eng*. 2016;8(4):521–532.
11. Li X, Feng Y, Gray KE. A hydro-mechanical sand erosion model for sand production simulation. *J Pet Sci Eng*. 2018;166:208–224.
12. Eshiet KII, Yang D, Sheng Y. Computational study of reservoir sand production mechanisms. *Geotech Res*. 2019;6(3):177–204.
13. Fetrati M, Pak A. Numerical simulation of sanding using a coupled hydro-mechanical sand erosion model. *J Rock Mech Geotech Eng*. 2020;12(4):811–820.
14. Van den Hoek PJ, Kooijman AP, De Bree P, Kenter CJ, Zheng Z, Khodaverdian M. Horizontal-wellbore stability and sand production in weakly consolidated sandstones. *SPE Drill Compl*. 2000;15(04):274–283.
15. Subbiah SK, Samsuri A, Mohamad-Hussein A, Jaafar MZ, Chen YR, Kumar RR. Root cause of sand production and methodologies for prediction. *Petroleum*. 2021;7(3):263–271.
16. Sarris E, Papaloizou L, Gravanis E. A hydro-mechanical constitutive law for modelling sand production. In: *55th US Rock Mechanics/ Geomechanics Symposium*. 2021.
17. Ma T, Qiu Y, Zhang Y, Liu Y. Numerical simulation of progressive sand production of open-hole completion borehole in heterogeneous igneous formation. *Int J Rock Mech Min Sci*. 2022;150:105030.
18. Zhang F, Wang T, Liu F, Peng M, Bate B, Wang P. Hydro-mechanical coupled analysis of near-wellbore fines migration from unconsolidated reservoirs. *Acta Geotech*. 2022;17(8):3535–3551.
19. Kakonitis P, Gravanis E, Sarris E. On the stress dependency of sand production coefficient in hydro-dynamical sanding criteria. *Int J Rock Mech Min Sci*. 2023;169:105443.
20. Stavropoulou M, Papanastasiou P, Vardoulakis I. Coupled wellbore erosion and stability analysis. *Int J Numer Anal Methods Geomech*. 1998;22(9):749–769.
21. Papamichos E, Vardoulakis I, Tronvoll J, Skjaerstein A. Volumetric sand production model and experiment. *Int J Numer Anal Methods Geomech*. 2001;25(8):789–808.
22. Nouri A, Vaziri H, Kuru E, Islam R. A comparison of two sanding criteria in physical and numerical modeling of sand production. *J Pet Sci Eng*. 2006;50(1):55–70.
23. Garolera D, Carol I, Papanastasiou P. Micromechanical analysis of sand production. *Int J Numer Anal Methods Geomech*. 2019;43(6):1207–1229.
24. Papamichos E. Analytical models for onset of sand production under isotropic and anisotropic stresses in laboratory tests. *Geomech Energy Environ*. 2020;21:100149.
25. Vardoulakis I, Stavropoulou M, Papanastasiou P. Hydro-mechanical aspects of the sand production problem. *Transp Porous Media*. 1996;22(2):225–244.
26. Fjaer E, Cerasi P, Li L, Papamichos P. Modeling the rate of sand production. In: *Gulf Rocks 2004, the 6th North America Rock Mechanics Symposium*. NARMS, 2004.
27. Detournay C. Numerical modeling of the slit mode of cavity evolution associated with sand production. *SPE J*. 2009;14(04):797–804.
28. Le Pense S. *Hydro-Mechanical Modelling of Damage-Plasticity Couplings in Unsaturated Geomaterials* (Doctoral Dissertation). Université Paris-Est; 2013.
29. Azadbakht S, Nouri A, Chan D. An analytical model for estimation of internal erosion rate. *Geomech Geoeng*. 2020;15(1):42–53.

30. Nouri A, Kuru E, Vaziri H. Elastoplastic modelling of sand production using fracture energy regularization method. *J Can Pet Technol*. 2009;48(04):64–71.
31. Vardoulakis IG, Sulem J. *Bifurcation Analysis in Geomechanics*. CRC Press; 1995.
32. Bratli RK, Risnes R. Stability and failure of sand arches. *Soc Pet Eng J*. 1981;21(02):236–248.
33. Morita N, Whitfill DL, Massie I, Knudsen TW. Realistic sand-production prediction: numerical approach. *SPE Prod Eng*. 1989;4(01):15–24.
34. Li HZ, Xiong GD, Zhao GP. An elasto-plastic constitutive model for soft rock considering mobilization of strength. *Trans Non-Ferrous Metals Soc China*. 2016;26(3):822–834.
35. Younessi A, Rasouli V, Wu B. Sand production simulation under true-triaxial stress conditions. *Int J Rock Mech Min Sci*. 2013;61:130–140.
36. Ouffroukh H. *Hydromechanical Behavior of the Granular Rock and Localization of the Deformation* (Doctoral Dissertation). Ecole des Ponts ParisTech; 2004.
37. Gravanis E, Sarris E, Patruno S. A simplified hydro-mechanical model for sanding from hollow cylinder tests. In: *56th US Rock Mechanics/Geomechanics Symposium*. 2022.
38. Kooijman AP, Van den Hoek PJ, De Bree P, Kenter CJ, Zheng Z, Khodaverdian M. Horizontal wellbore stability and sand production in weakly consolidated sandstones. In: *SPE Annual Technical Conference and Exhibition*. OnePetro; 1996.